XAS Investigation of the Structure and Function of Ni in Acireductone Dioxygenase†

Faizah Al-Mjeni,‡,|| Tingting Ju,§ Thomas C. Pochapsky,§ and Michael J. Maroney*,‡

Department of Chemistry, University of Massachusetts, Amherst, Massachusetts 01003-9336, and Department of Chemistry, Brandeis University, Waltham, Massachusetts 02454-9110

Received December 28, 2001; Revised Manuscript Received April 5, 2002

ABSTRACT: Acireductone dioxygenases (ARDs) are enzymes involved in the methionine recycle pathway, which regulates aspects of the cell cycle. *Klebsiella pneumoniae* produces two enzymes that share a common polypeptide sequence and differ only in the metal ion present. Reaction of acireductone (1,2-dihydroxy-3-keto-5-methylthiopentene) with Fe-ARD and dioxygen produces formate and 2-keto-4-methylthiobutanoic acid, the α-ketoacid precursor of methionine. Ni-ARD reacts with acireductone and dioxygen to produce methylthiopropionate, CO, and formate and does not lie on the methionine recycle pathway. An X-ray absorption spectroscopy (XAS) study of the structure of the catalytic Ni center in resting Ni-ARD enzyme and the enzyme−substrate complex is reported. This study establishes the structure of the Ni site in resting Ni-ARD as containing a six coordinate Ni site composed of O/N-donor ligands including 3−4 histidine residues, demonstrates that the substrate binds to the Ni center in a bidentate fashion by displacing two ligands, at least one of which is a histidine ligand, and provides insight into the mechanism of catalysis employed by a Ni-containing dioxygenase. Efficiently relaxed and hyperfine-shifted resonances are observed in the ^{1}H nuclear magnetic resonance spectrum of Ni-ARD that can be attributed to the His imidazoles ligating the paramagnetic Ni ion and are consistent with the XAS results regarding His ligation. These resonances show significant perturbation in the presence of substrate, confirming that the metal ion interacts directly with the substrate.

Polyamines are molecules that are critical for proper regulation of the cell cycle. The addition of polyamines to cells accelerates their DNA replication and division, whereas inhibition of polyamine biosynthesis arrests DNA replication and prevents continuation of the cell cycle (*1*). Methylthioadenosine (MTA), a derivative of *S*-adenosylmethionine (AdoMet), is a strong inhibitor of polyamine biosynthesis and transmethylation reactions (*2*). The concentration of MTA in biological systems is therefore tightly regulated. This control is achieved through the methionine salvage pathway, where MTA is recycled through a series of reactions that convert its 5-methylthio-D-ribose moiety to methionine (Scheme 1) (*3*).

The methionine salvage pathway has been identified in many organisms. In *Klebsiella pneumoniae*, where the pathway has been investigated in detail, all of its intermediates have been identified (Scheme 1) (*4*). Acireductone (1,2-dihydroxy-3-keto-5-methylthiopentene) is an intermediate in the methionine salvage pathway. Two enzymes have been identified in *K. pneumoniae* that catalyze the oxidation of acireductone, both of which are known as acireductone dioxygenases (ARDs, Scheme 1) (*5*).[1] The products of the two enzymatic acireductone oxidations differ in that one enzyme (Fe-ARD or ARD′) converts acireductone to the α-ketoacid precursor of methionine and formate, while the other enzyme (Ni-ARD or ARD) produces methylthiopropionate, CO, and formate and does not recycle MTA to methionine (*4*−*6*). Previous work has established that the two ARDs can be separated by ion exchange chromatography but are derived from the same protein and differ only in their metal content (*5*). Both enzymes are obtained upon overexpression of a single open-reading frame in *Escherichia coli*; the apoproteins are identical 20.2 kDa polypeptides, and the activities of the two enzymes are interconverted by exchanging Fe and Ni (*5*). Thus, Fe-ARD and Ni-ARD represent the only characterized pair of naturally occurring metalloenzymes with distinct chemical and physical properties determined solely by metal ion content.

Ni-ARD is also the only example of a Ni-containing dioxygenase. The precise function of the Ni-ARD reaction in the *K. pneumoniae* is unclear. Its products are not precursors for methionine, and methylthiopropionic acid is cytotoxic (*7*). The Ni-ARD-catalyzed reaction may thus be considered a shunt in the methionine salvage pathway, aiding in the regulation of methionine. Alternatively, CO, a product of the Ni-ARD reaction, has recently been identified as a

† Supported by the University of Massachusetts (M.J.M.) and by NIH Grant R01-GM44191 (T.C.P.).

* To whom correspondence should be addressed. Department of Chemistry, Lederle Graduate Research Center, 710 North Pleasant St., University of Massachusetts, Amherst, MA 01003-9336. Tel.: 413-545-4876. Fax: 413-545-4490. E-mail: mmaroney@chem.umass.edu.

‡ University of Massachusetts.

§ Brandeis University.

|| Department of Chemistry, College of Science, Sultan Qaboos University, P.O. Box 36, Al-Khod, PC 123, Sultanate of Oman.

[1] Abbreviations: ARD, acireductone dioxygenase; EXAFS, extended X-ray absorption fine structure; XANES, X-ray absorption near-edge structure; XAS, X-ray absorption spectroscopy.

10.1021/bi012209a CCC: $22.00
Published on Web 05/03/2002

Scheme 1

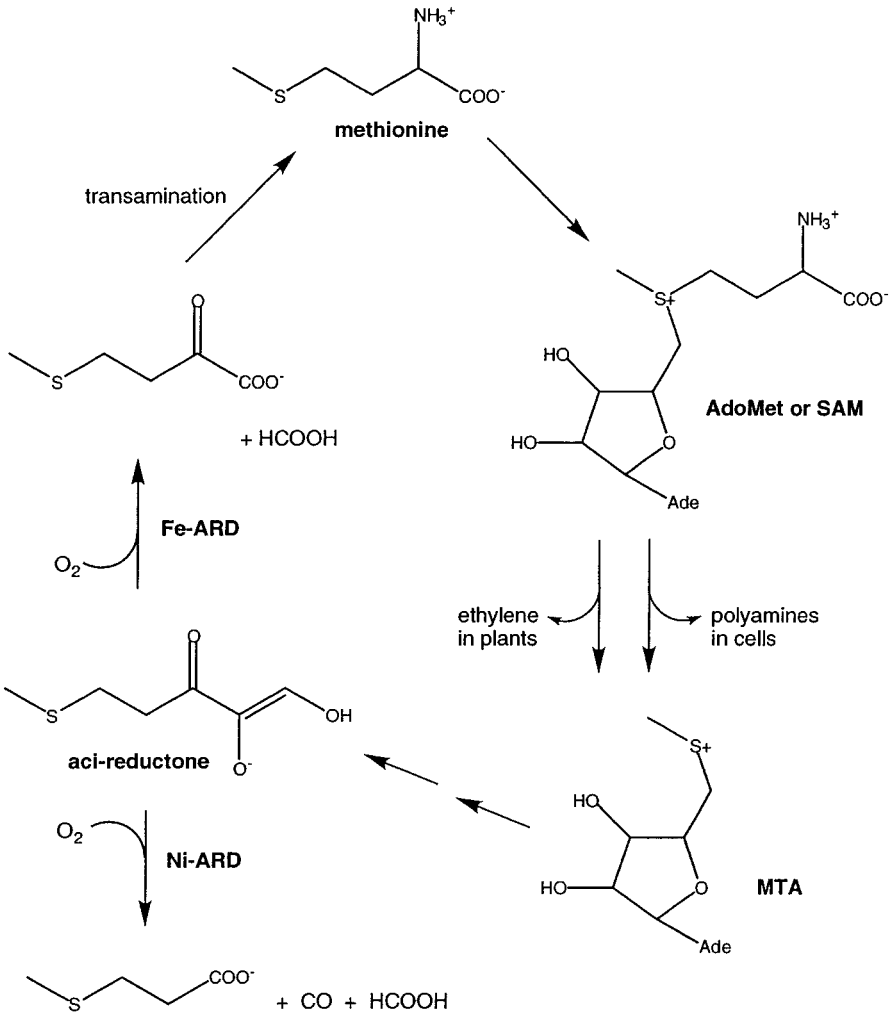

neurotransmitter in mammals and might play a role as a diffusible messenger in *K. pneumoniae* (*8*, *9*). Here, we present an X-ray absorption spectroscopy (XAS) study of the structure of the catalytic Ni center in resting Ni-ARD enzyme and the enzyme−substrate (ES) complex. This study establishes the structure of the Ni site in the resting enzyme as containing a six coordinate Ni site composed of O/N-donor ligands including 3−4 histidine residues, demonstrates that the substrate binds to the Ni center in a bidentate fashion by displacing two ligands, at least one of which is a histidine ligand, and provides insight into the mechanism of catalysis employed by a Ni-containing dioxygenase.

MATERIALS AND METHODS

Expression and Purification of ARD. The plasmid vector used for expression of ARD is derived from pET19b, a commercially available T7 RNA polymerase-based expression system (Novagen). The ARD gene is inserted between BamHI and NdeI restriction sites of the pET19b plasmid. The cloning and overexpression of ARD has been described (*5*). All purification steps were performed at 4 °C unless otherwise noted. BL21(DE3)(pLys) *E. coli* cells were electroporated and transformed with the appropriate plasmid. After growth on agar overnight with the appropriate antibiotic selection (chloroamphenicol and ampicillin), single colonies were inoculated into 5 mL cultures in Luria−Bertani broth supplemented with chloroamphenicol (34 mg/L) and ampicillin (200 mg/L). As soon as viable cultures were established to the eye, 100 μL of the cultures was inoculated into M9 minimal media (6 g/L Na_2HPO_4, 3 g/L KH_2PO_4, 1 g/L NH_4-Cl, 0.5 g/L NaCl, 0.0005% thiamine, 0.4% glucose, 0.8 mM $MgSO_4$, trace metal supplements, 200 mg/L ampicillin, and 34 mg/L chloroamphenicol). When an optical density of 0.5 was reached, the media were supplemented with $NiCl_2$ (1 μM), and IPTG (isopropyl-β-thiogalactoside) was added to a final concentration of 0.3 mM. After stationary phase was reached, cells were harvested by centrifugation and frozen at −70 °C for several days. The cells were then thawed in 8 volumes (w/v) of 50 mM TrisHCl buffer (pH 8.0). The suspension was sonicated 6 × 45 s with a Fisher sonic dismembrator model 300 at 75% maximal output. To every 100 mL of sonicate, 10 mg of DNAase I, 6 mg of RNAase A, and 20 mg of tosyl chloride were added. The mixture was stirred for 30 min, and then, the sonicate was centrifuged at 20 000*g* for 60 min. The pellet was discarded. To the supernatant liquid, finely ground ammonium sulfate was added slowly with stirring to a concentration of 40% w/v (22.6 g/100 mL). The subsequent suspension was stirred for 30 min, and the precipitate was removed by centrifugation at 30 000*g* for 20 min. The pellet was discarded, and the concentration of ammonium sulfate in the supernatant liquid was increased to 55% w/v (another 8.9 g/100 mL). After 30 min of stirring, the precipitate was again collected by centrifugation at 30 000*g* for 20 min. At this stage, a sodium

dodecyl sulfate (SDS) gel was performed to confirm that most of the ARD was in the 55% ammonium sulfate pellet. The ARD pellet was resuspended in a minimal amount of 20 mM TrisHCl buffer (pH 7.4) and dialyzed against 20 mM TrisHCl buffer (pH 7.4) overnight. The protein solution was centrifuged at 10 000*g* for 5 min, and the precipitate was discarded. The ARD in the clarified dialysate was then purified using a BioCAD SPRINT FPLC system over a MonoQ 10/10 anion exchange column (Amersham). The protein was eluted from the column by linear salt gradient, increasing NaCl concentration from 0 to 150 mM over 80 mL, followed by another linear gradient of NaCl increasing concentration from 150 to 300 mM over 240 mL. ARD eluted in the fraction(s) that had a NaCl concentration of 160 mM. Protein purity was established by SDS−polyacrylamide gel electrophoresis (PAGE) gel, and concentrations were established by nuclear magnetic resonance (NMR) and UV−visible spectroscopy.

XAS and NMR Sample Preparation. ARD samples for XAS were prepared by dialysis against 10 mM Tris acetate (pH 7.4). After dialysis, the samples were concentrated to 1 mM. The sample (50−60 μL) was transferred to an extended X-ray absorption fine structure (EXAFS) sample holder and frozen on dry ice. For XAS samples containing substrate, a buffered solution of 100 mM substrate precursor 1-phosphato-2,3-diketohexane was treated anaerobically with a catalytic quantity of enolase-phosphatase E1 and $MgCl_2$ (*6*). After 0.5 h, 10 μL of the substrate solution was mixed anaerobically with the ARD sample and frozen into XAS sample holders as described above. NMR samples of ARD with and without substrate were prepared in a similar manner, except 10 mM d-TrisCl (pH 7.4) in 90/10 H_2O/D_2O was used as a buffer.

XAS Methods. XAS data for all samples were acquired at beamline X9B at the National Synchrotron Light Source (NSLS) at the Brookhaven National Laboratory during several sessions. The samples were contained in polycarbonate holders that were inserted into a slotted aluminum holder and held near 50 K using a He displex cryostat. The XAS data were collected under dedicated conditions at ca. 2.8 GeV and 160−260 mA as previously described (*10*), except that a sagitally focusing Si(111) double-crystal monochromator was used for these studies. The X-ray energy of the focused monochromatic beam was internally calibrated to the first inflection point of Ni foil (8331.6 eV).

X-ray fluorescence data were collected using a 13 element Ge detector (Canberra). X-ray absorption near-edge structure (XANES) data were collected over the range from ca. 8100−8500 eV, with the vertical primary aperture reduced to 0.3 mm. Harmonic rejection was achieved by use of a Ni mirror. This arrangement gives a theoretical energy resolution of ca. 3 eV and gave spectral resolution comparable to that obtained on model compounds using a flat Si(220) double-crystal monochromator at this beam line, as previously described (*10*). The spectral features are reproducible to within 0.2 eV in sequential scans. EXAFS data were collected over a scan range from 8100 to 9400 eV under the same conditions used for collection of XANES data except that the vertical primary aperture was set at 1.0 mm. This arrangement results in lower energy resolution (ca. 5 eV) but provides higher X-ray beam intensity.

The integrity of the samples during ~10 h of exposure to monochromatic synchrotron radiation was determined by monitoring the Ni−K edge energy on sequential scans. No changes in either edge energy (redox state) or pre- or post-edge XANES spectra (ligand environment) were observed. In addition, electron paramagnetic resonance (EPR) spectra of the samples were acquired before and after exposure to synchrotron radiation, to monitor any changes in the Ni^{2+} oxidation state. The samples did not exhibit any Ni-based EPR signals before or after exposure, although exposed samples did show a signal associated with the production of solvated electrons during exposure to synchrotron radiation. Activity assays performed after exposure to synchrotron radiation show that the enzyme did not suffer a significant loss in activity (same order of magnitude).

The average of 11 scans (143 spectra) for resting Ni-ARD and 3 scans (39 spectra) for Ni-ARD ES complex were used for XANES analysis. The Ni−K edge energies reported were taken to be the energy at a normalized intensity of 0.5. The peaks in pre-edge XANES spectra at ca. 8332 eV peaks are assigned to 1s → 3d electronic transitions. The area of these peaks was determined by fitting a baseline to the region of the normalized spectrum immediately below and above this feature in energy and integrating the difference (*11*).

EXAFS data were analyzed using WinXAS (*12*). The average of 15 scans (195 spectra) for resting Ni-ARD and 12 scans (156 spectra) for the Ni-ARD ES complex were used for EXAFS analysis. The summed, energy-calibrated data files were background-corrected and normalized using a two polynomial fit, with a first-order polynomial for the pre-edge region and a third-order polynomial for the post-edge region. The data were converted to k space using the relationship $[2m_e(E - E_0)/\hbar^2]^{1/2}$ (where m_e is the electron mass, E is the photon energy, $\hbar$ is Planck's constant divided by 2π, and E_0 is the threshold energy of the absorption edge and defined here as 8340.0 eV). A least-squares fitting procedure was employed over a k range of 2−12.5 $Å^{-1}$ using Fourier-filtered EXAFS with a back transform window of 1.1−4.2 Å (uncorrected for phase shifts). The presence of trace amounts of Cu in the samples required the data be truncated at $k = 12.5$ $Å^{-1}$. The fitting procedure minimized $\mathrm{GOF} = 1/\sigma^2 \sum_{i=1}^{N}[y_{exp}(i) - y_{theo}(i)]^2$ (where σ is an estimate of the experimental error and y_{exp} and y_{theo} are experimental and theoretical data points, respectively, and N is the number of data points) (*12*). Comparison of residual values (*12*) (eq 1) and the difference in the disorder parameters between theoretical model data and the fit, $|\Delta\sigma^2| = |(\sigma^2_{fit} - \sigma^2_{theory})|$, using the EXAFS formula (eq 2) (*12*) were used to select the best fits of the data.

$$\text{residual (\%)} = \frac{\sum_{i=1}^{N}|y_{exp}(i) - y_{theo}(i)|}{\sum_{i=1}^{N}|y_{exp}(i)|} \times 100 \quad (1)$$

$$\chi(k) = \sum_j \frac{N_j S_0^2 F_j(k)}{kR_j^2} \times e^{(-2k^2\sigma_j^2)} \times e^{(-2R_j/\lambda)} \times \sin[2kR_j + \delta_j(k)] \quad (2)$$

Theoretical phases and amplitudes for EXAFS analyses were obtained from FEFF 6 using the crystallographically characterized model compounds diaqua-bis(salicylaldehydato) nickel(II) (*13*), $[Ni(sal)_2(H_2O)_2]$, $[Ni(Im)_6](BF_4)_2$ (*14*), tetraethylammonium tetrakis (*p*-chlorobenzenethiolato) nickelate(II) (*15*), and $(Et_4N)_2[Ni(p\text{-}SC_4H_4Cl)_4]$ as previously described (*16*). The phase and amplitude parameters from the calculations were then used to fit data obtained on the same model compounds used in the calculations in order to obtain values for σ_{model} and E_0. The EXAFS analysis of Ni-ARD data was carried out as previously described (*16*). The value of E_0 determined from fitting model compounds was held constant for each shell of scattering atoms. Integer values for the number of scattering atoms in a shell were used in the fits without refinement. This led to two free-running parameters (N_{frp}) for each shell in the first coordination sphere: the distance (r) and the disorder parameter (σ^2). The EXAFS arising from histidine imidazole ligands was fit using multiple scattering analysis. Only those scattering pathways with a relative intensity >17% were used in the data analysis in order to limit the number of free-running parameters used in the fits. To further limit the number of adjustable parameters, the imidazole ligands were assumed to be symmetrically bound (identical Ni−X distances, where X is a second coordination sphere C atom or third coordination sphere C- or N-atom), and a single value of σ^2 was used to describe the atoms in each coordination sphere. Imidazole ligands were "counted" by adding rings as integer units and examining the residual and σ^2 values in the fits. The distances reported are the distances obtained from the relevant single-scattering pathway. Using these procedures, refined distances (fitting EXAFS frequencies) to atoms in the first coordination sphere of model complexes were within ±0.02 Å of crystallographic distances, and distances for second and third coordination sphere atoms were within ±0.04 Å. The number of scattering atoms in a shell, or the number of imidazole rings (fitting EXAFS intensity), is accurate to ±25%.

^{1}H NMR Spectroscopy of Substrate-Free and Substrate-Bound Ni-ARD. NMR experiments were performed on a Varian Unity 500 NMR spectrometer operating at 500.139 MHz (^{1}H) at Brandeis University. A 300 μL amount of a 1 mM sample of Ni-ARD in 90/10 H_2O/D_2O (10 mM d-tris HCl, pH 7.4) was placed in a susceptibility-matched NMR tube (Shigemi). A ^{1}H NMR spectrum was acquired at 25 °C with a wide (125 kHz) spectral width and a short delay (100 ms) between acquisitions in order to suppress diamagnetic resonances. The spectra are an average of 2048 scans. The intense water signal was removed either by presaturation with a low power (100 Hz) RF pulse during the 100 ms delay or by setting the carrier frequency at 60 ppm and using an excitation pulse of appropriate amplitude and duration to place a null at the water frequency. Hydrogen/deuterium exchange was accomplished by lyophilization of the ARD sample twice, in each case followed by solution of the dried sample with D_2O. Substrate (nominally 10 mM) was added to ARD anaerobically as described above for XAS experiments for comparison of the substrate-free and substrate-bound Ni-ARD spectra. The appearance of bubbles after time (presumably of CO) indicated that turnover was occurring in the NMR tube, so the actual concentration of substrate is less than nominal concentration introduced. Data were processed with a 50 Hz line broadening and a cubic spline baseline correction.

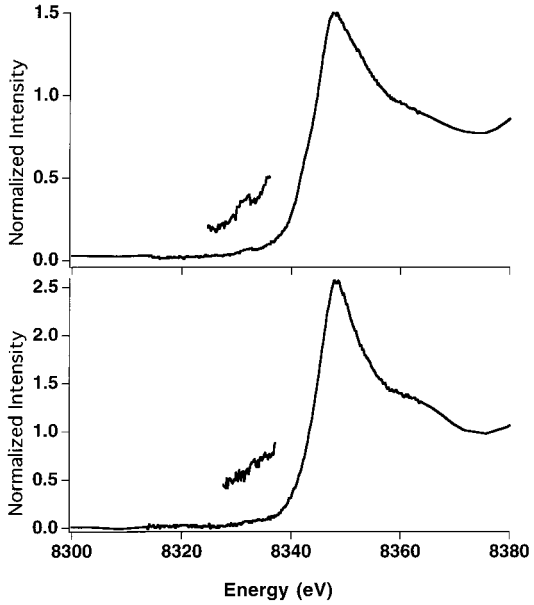

FIGURE 1: Ni−K edge XANES of the resting (top) and the ES complex (bottom) of *K. pneumoniae* Ni-ARD. Inserts show an expansion of the region around 8332 eV, where the 1s → 3d transition is expected.

RESULTS

XANES Analysis. The Ni−K edge XANES spectra obtained for Ni-ARD and Ni-ARD ES complex are compared in Figure 1. The pre-edge, edge, and post-edge analyses are consistent with six coordinate Ni centers with primarily O/N-donor ligands in both cases. The pre-edge features show small 1s → 3d peaks near 8332 eV, with peak areas of $2.8(2) \times 10^{-2}$ eV for the resting enzyme and $3.0(4) \times 10^{-2}$ eV for the ES complex. These values fall in the range appropriate for centrosymmetric (six coordinate or four coordinate planar) Ni^{2+} complexes (*11*). Neither spectrum shows a resolved peak near 8338 eV (assigned to a 1s → $4p_z$ transition with shakedown contributions) that is diagnostic for planar, four coordinate Ni centers (*11*, *17*). The lack of a peak or shoulder near 8338 eV effectively rules out the possibility that either of these samples contains four coordinate planar or square pyramidal five coordinate Ni centers.

Resting Ni-ARD has an edge energy of 8341.6(2) eV, and the ES complex has an edge energy of 8341.2(2) eV. Both of these values are appropriate for Ni^{2+} centers in O/N coordination environments. The shift of −0.4 eV produced on substrate binding suggests a small increase in the electron density of the Ni center when the substrate is bound. The magnitude of the shift indicates that it results from a change in the ligand environment of the nickel, rather than a redox state change, since a one electron metal-centered redox reaction would result in a 2−3 eV energy shift, assuming a static ligand environment (*11*). Thus, no redox change occurs upon substrate binding.

The white line intensity (the highest absorption in the XANES spectrum, Figure 1) is another indication of the type of ligands bound to the nickel. The intensity of this feature, relative to the normalized edge, is an indication of whether

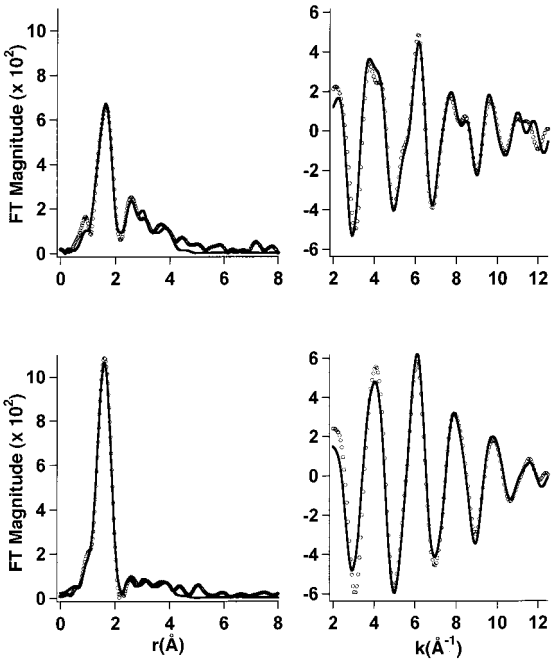

FIGURE 2: Ni−K edge Fourier-transformed (k = 2−12.5 Å^{-1}) EXAFS spectra (left), and Fourier-filtered (back transform window = 1.1−4.2 Å) EXAFS spectra (right) of the resting (top) and the ES complex (bottom) of *K. pneumoniae* Ni-ARD. Data points are represented by open circles (○) and the fita by a solid line (−). The fits shown for the resting Ni-ARD and the ES complex are fits R09 and ES06 from Table 1, respectively.

the active site Ni has ionic (hard donor atoms such as N/O) or a more covalent binding (soft ligands such as RS^-/Cl^-). In the XANES of the Ni-ARD resting and ES complex, the white line indicates a more ionic binding and thus a predominance of hard, N/O-donors (*11*).

EXAFS Analysis. The EXAFS spectra for resting Ni-ARD and the Ni-ARD ES complex are compared in Figure 2. Visual inspection of the data reveals that the spectrum changes when substrate is added, implying that the substrate binds to the Ni site. One of the changes that occurs is a dramatic decrease in the intensity of features in the Fourier-transformed spectrum at a radial distance of ca. 3−4 Å (uncorrected for phase shifts) in the spectrum of ES complex. These features are generally attributable to the presence of histidine imidazole ligands; thus, inspection of the spectra suggests the displacement of one or more histidine ligands when substrate binds. The curve-fitting analyses of the EXAFS data presented in Table 1 corroborate these results and provide metric details regarding the Ni sites.

The best single shell fit of the resting enzyme contains five or six O/N-donor ligands. Although it is not generally possible to distinguish O- and N-donors from EXAFS analysis alone, the use of six N-atoms gave fits that are about 20% better than obtained using six O-parameters, and no acceptable fits were obtained using S-atoms to model the first-coordination sphere (see Supporting Information). The fit using five N-atoms to model the first coordination sphere (R01) has a slightly better residual and a lower disorder than the six coordinate fit (R02). However, several facts favor the six coordinate fit: First, because of correlation between the number of scattering atoms and their disorder, the error in the number of scatters determined by fitting EXAFS intensity is ∼±25%. Second, the XANES analysis is most consistent with a six coordinate Ni site. Third, bond−valence−sum (BVS) analysis gives an unacceptably low value of the oxidation state of Ni when the information from the EXAFS fits of five coordinate structures is used in the calculation. BVS is an empirical method that can be used to verify the compatibility of the metal−ligand bond distances in the structural model to that of the metal's oxidation state (*18*). In the case of resting Ni-ARD, the metal ion present is Ni^{2+} and fits with five first-coordination sphere ligands give BVS values that are below the ±0.25 error limits accepted for BVS analysis (*18*).

The large disorder for the six first-coordination sphere N-donors in the single shell fit suggests that the first-coordination sphere might contain two distinct shells of scattering atoms. Fits obtained using either two shells of N-donors or mixed shells (one shell of O-atoms and one shell of N-atoms) give comparable fits that have a modest improvement in the residual. The best two-shell fit (R05) features one O-donor at 1.91(2) Å and five N-donors at 2.10(2) Å, improves the residual by 11%, and gives typical disorder parameters for both shells. Large improvements in the residual (e.g., 72% for R05 vs R09) are obtained by modeling 3−4 of the first-coordination sphere ligands as histidine imidazole rings (fits R07−R10). Fits obtained with three His ligands generally have slightly poorer residuals but better disorder parameters than fits obtained with four His ligands. On the basis of the Ni−O distance and the multiple scattering analysis, the Ni site in the resting enzyme is best described as containing six O/N-donors, one of which is likely an O-atom at a shorter 1.91 Å distance and 3−4 of which are His ligands.

The fits obtained for the Ni-ARD ES complex show the nature of the structural change that occurs when substrate binds to the Ni site. The coordination number of the Ni center remains the same in both enzymes (from XANES analysis), and the EXAFS data for the Ni center in the ES complex are best fit by six O/N-scattering atoms having acceptable disorder parameters. In the case of the Ni-ARD ES complex, single-shell fits using six O-atoms gave results that are about 30% better than those using six N-atoms (see Supporting Information), suggesting that there are more O-donors in the ligand environment of the Ni center relative to the resting enzyme. Splitting the shell into two shells of scatterers at different distances does not improve the residual much (7%); thus, the first coordination sphere is modeled fairly well by six O/N-donors at 2.04(2) Å ave. Ni−L distance (ES01). Splitting the first coordination sphere into two shells gives many combinations of two shells of O-atoms and mixed O/N-shells with comparable fits (see Supporting Information). However, only one of the best two-shell fit gives an acceptable value for the BVS (ES03, BVS = 2.17). This fit consists of four O-donors with Ni−O distances of 2.00(2) Å and two N-donor ligands at 2.14(2) Å. All other acceptable two-shell fits have more O-scattering atoms and result in a BVS ≥2.25 (e.g., ES02). This suggests that at least two of the ligands must be N-donor ligands.

The presence of N-donor ligands in the Ni-ARD ES complex is confirmed by multiple scattering analysis. Modeling 1−2 of the first coordination sphere O/N-donor ligands as His imidazole ligands leads to substantial improvements in the residuals of the fits (50% for single shell vs single shell + 1−2 imidazoles). Fits obtained with two His ligands

Table 1: Selected Fits from the Curve-Fitting Results of Fourier-Filtered EXAFS Spectra of the *K. pneumoniae* Ni-ARD Resting Enzyme and ES Complex[a]

sample/fit no.	*N*	*r* (Å)	σ^2 ($\times 10^3$ Å^2)	$\Delta\sigma^2$ ($\times 10^3$ Å^2)	N_{frp}/N_{idp}	% residual	BVS
			Resting				
R01	5	Ni − N = 2.0728(3)	8.4	3.8	2/22	37.0	1.59
R02	6	Ni − N = 2.0736(3)	*10.5*	5.9	2/22	37.1	1.91
R03	4	Ni − N = 2.0176(6)	9.6	5.0	4/22	33.4	1.99
	2	Ni − N = 2.135(1)	2.7	−1.9			
R04	3	Ni − N = 1.9927(7)	7.9	3.3	4/22	33.4	2.00
	3	Ni − N = 2.1251(8)	3.8	−0.8			
R05	5	Ni − N = 2.0959(4)	6.8	2.2	4/22	33.2	1.99
	1	Ni − O = 1.912(1)	4.9	0.3			
R06	4	Ni − N = 2.1169(5)	5.5	0.9	4/22	33.4	2.05
	2	Ni − O = 1.9485(7)	6.9	2.3			
R07	6	Ni − N = 2.0712(3)	*10.4*	5.8	9/22	12.6	1.91
	3(His)	Ni − C = 3.0644(7)	5.9	0.4			
		Ni − C/N = 4.197(6)	7.7	2.2			
R08	6	Ni − N = 2.0706(3)	*10.4*	5.8	9/22	11.3	1.91
	4(His)	Ni − C = 3.0650(6)	7.4	1.9			
		Ni − C/N = 4.198(4)	*10.8*	5.3			
R09	1	Ni − O = 1.905(1)	6.7	2.1	11/22	9.2	2.03
	5	Ni − N = 2.0892(4)	7.1	2.5			
	3(His)	Ni − C = 3.0676(7)	5.8	0.3			
		Ni − C/N = 4.177(5)	8.6	3.1			
R10	1	Ni − O = 1.905(1)	7.1	2.5	11/22	8.4	2.03
	5	Ni − N = 2.0882(5)	7.1	2.5			
	4(His)	Ni − C = 3.0689(6)	7.4	1.9			
		Ni − C/N = 4.198(4)	*10.5*	5.0			
			ES Complex				
ES01	6	Ni − O = 2.0383(4)	7.6	3.0	2/22	15.9	2.20
ES02	4	Ni − O = 1.9977(1)	6.6	2.0	4/22	14.8	2.28
	2	Ni − O = 2.0927(3)	3.2	−1.4			
ES03	2	Ni − N = 2.1364(2)	1.9	−2.7	4/22	14.8	2.17
	4	Ni − O = 2.0008(1)	4.9	0.3			
ES04	6	Ni − O = 2.0337(1)	7.6	3.0	9/22	8.4	2.27
	1(His)	Ni − C = 3.0809(5)	8.2	2.7			
		Ni − C/N = 4.253(8)	5.7	0.2			
ES05	6	Ni − O = 2.0336(1)	7.6	3.0	9/22	8.0	2.27
	2(His)	Ni − C = 3.0889(4)	*12.7*	7.2			
		Ni − C/N = 4.256(1)	8.0	2.5			
ES06	2	Ni − N = 2.1352(2)	1.7	−2.9	11/22	7.6	2.17
	4	Ni − O = 1.9998(1)	5.0	0.4			
	1(His)	Ni − C = 3.1016(3)	4.7	−0.8			
		Ni − C/N = 4.28(2)	3.2	−2.3			
ES07	2	Ni − N = 2.1337(2)	1.9	−2.7	11/22	7.4	2.18
	4	Ni − O = 2.0003(1)	5.1	0.5			
	2(His)	Ni − C = 3.1085(3)	8.9	3.4			
		Ni − C/N = 4.175(2)	*10.2*	4.7			

[a] Fourier transform limits: $k = 2-12.5$ Å^{-1}; back transform window = 1.1−4.2 Å; *N* is the number of bonds at a specific distance; *R* (Å) is the bond distance; σ^2 is the root mean square disorder in the bond distance; $\Delta\sigma^2$ is σ^2 relative to calculated values for reference compounds, $|\Delta\sigma^2| = |(\sigma^2_{fit} - \sigma^2_{model})|$; N_{frp} is the number of free-running parameters in the fit; N_{idp} is the number of independent data points; and residual is calculated as described in the Experimental Section. The accuracy of distances determined by EXAFS for atoms in the first coordination sphere of the metal are limited to ±0.02 Å by the theoretical phase parameters. The refinements generally show precisions that are less than 0.02 Å for well-ordered shells; thus, differences in distances between samples using equivalent fits are more accurate than the absolute distances. The distances shown are for the single scattering pathways. Large values of σ^2 (underlined) suggest that the shell involved has a coordination number that is too large or is badly disordered. BVS = Σs, where *s* is calculated by the equation $s = \exp((r_0 - r)/0.37)$, (*18*); r_0 values were obtained from published tables (*18*), and *r* is the bond distance, *R* (Å), as determined from EXAFS analysis.

gave slightly lower residuals but had larger disorder parameters than fits obtained using only one His ligand. On the basis of the analysis above, the best description of the Ni site in Ni-ARD ES complex is that it contains six O/N-donor ligands, of which one or two are His ligands.

^{1}H NMR Results. Figure 3 shows a comparison of paramagnetically shifted and broadened resonances in the downfield region of the ^{1}H NMR spectrum in D_2O (top), in H_2O (middle), and in H_2O with added substrate (bottom). The pattern of resonances in the region between 72 and 48 ppm as well as their hydrogen−deuterium exchange behavior show a remarkable parallel with that of the His-ligated Ni(II)-bound form of the HNH motif of colicin E9 (*19*). There is a crystal structure available for this protein, and it allowed those investigators to assign the signals observed in this region of the Ni-binding protein to the imidazole ring protons of the ligating His residues that are further than ~5 Å from the bound Ni (*20*). In the case of ligation of the Ni through the $N_{\delta1}$ position of the His imidazole, this would include two protons, an exchangeable ($N_{\epsilon2}H$) and a nonexchangeable ($C_{\delta2}H$) proton. If the Ni is ligated through the $N_{\epsilon2}$ imidazole nitrogen, only the exchangeable $N_{\delta1}$ proton would be observed. Like ARD, exchange of the NHN domain of colicin E9 into D_2O resulted in the loss of three of the four

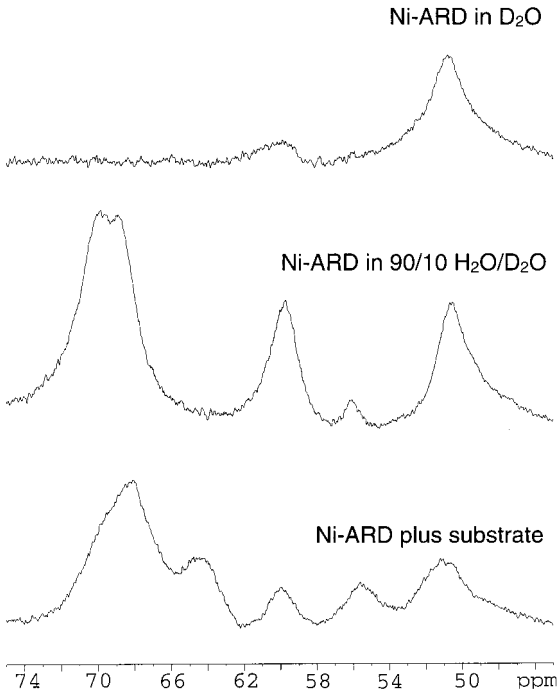

FIGURE 3: Hyperfine-shifted resonances in the 11.74 T (500 MHz) ^1H NMR spectra of 1 mM Ni-ARD in 100% D_2O (pH 7.4 d-tris 10 mM) (top), 1 mM Ni-ARD in 90/10 H_2O/D_2O (pH 7.4 d-tris 10 mM) (middle), and 90/10 H_2O/D_2O (pH 7.4 d-tris 10 mM) with 10 mM substrate added (bottom, see Experimental Section for details). All spectra were obtained at 298 K.

major signals between 74 and 48 ppm, consistent with the X-ray crystallographic result that the Ni(II) in the NHN domain is ligated by three His imidazoles, two via the $N_{\epsilon 2}$ nitrogens and one via the $N_{\delta 1}$ nitrogen.

In the present case, sequence homology of the ARD gene from *K. pneumoniae* with putitive ARD genes from *Homo sapiens*, *Oryza sativa*, and *Pseudomonas aurigenosa* identifies three His residues, His96, His98, and His140, that are conserved in all four sequences and are not observed in the diamagnetic NMR spectra of Ni-ARD (*21*). Combined with the XAS data presented here, the NMR results confirm that the Ni(II) in ARD is ligated by three His residues. Furthermore, the observed H/D exchange pattern shown in Figure 3 suggests that ligation of the Ni(II) by two of those His is through the $N_{\epsilon 2}$ nitrogen and through the $N_{\delta 1}$ in the third.

Upon addition of substrate (bottom spectrum), several new resonances appear, at 55 and 65 ppm, with some evidence for a broader resonance at 40 ppm. It is impossible to make any definitive interpretation of these perturbations, as the overall stoichiometry of the mixture could not be established with certainty due to some adventitious turnover of substrate. However, it is clear from the data that the metal center is interacting directly with the substrate and that this results in some perturbation of the His ligands. This is consistent with the XAS results that indicate the loss of at least one His ligand when substrate binds. We are currently using isotopic labeling methods to investigate these perturbations in more detail.

DISCUSSION

Ni-ARD is the only characterized example of a Ni-containing dioxygenase. The apparent biological role of Ni-ARD is to provide a shunt out of the methionine salvage pathway, which may serve as a mechanism for regulating methionine levels (Scheme 1) (*22*). It is also possible that the CO produced by Ni-ARD catalysis serves a signal function in *K. pneumoniae* cultures (*8*, *9*). The enzyme is also unique in that substitution of Ni^{2+} by Fe^{2+} yields another enzyme with an altered product distribution and physical properties (*4*−*6*). Fe-ARD produces a product that upon transamination yields methionine and does not produce CO (Scheme 1). Both enzymes can be isolated from *K. pneumoniae* or by expression of a single *K. pneumoniae* open-reading frame in *E. coli* (*5*).

The mechanism of catalysis utilized by Ni-ARD has been examined by a series of experiments utilizing acireductone, ^{14}C-labeled substrate or substrate analogues, and $^{18}O_2$ (*4*, *22*, *23*). These experiments establish that Ni-ARD is a dioxygenase (one O-atom is incorporated into the formate and one into the carboxylic acid moiety; none is found in CO), demonstrate that CO is derived from C2, and are consistent with a sequential mechanism in which formation of a ternary complex (ESO_2) involving substrate binding prior to O_2 binding is required before product release.

The ionic state of acireductone bound to Ni-ARD has also been examined (*22*). On the basis of titrations of the substrate analogue 1,2-dihydroxy-3-keto-1-hexene, the α-keto enediol functional group in acireductone is expected to have pK_a values near 4.0 and 12.2. Thus, acireductone is a monoanion at neutral pH. The electronic absorption spectrum of α-keto enediols depends on its protonation state. The spectrum obtained from 1,2-dihydroxy-3-keto-1-hexene at pH 7.4 features a $\lambda_{max} = 305$ nm that shifts to 345 nm at pH 13. Under anaerobic conditions, binding of 1,2-dihydroxy-3-keto-1-hexene to Ni-ARD is accompanied by a red shift in the λ_{max} from 305 to 345 nm, demonstrating that the substrate analogue is bound to the enzyme as a dianion containing an α-keto enediolate moiety. Thus, a basic amino acid is used to deprotonate the monoanionic substrate to form the ES complex.

The reaction products found in the studies using labeled substrates and $^{18}O_2$ are consistent with attack of O_2 at C1 and formation of a five-membered cyclic peroxo intermediate (Scheme 2) (*4*, *22*, *23*). It was suggested that the difference between Fe-ARD and Ni-ARD may lie in the formation of a four-membered cyclic peroxide in Fe-ARD vs a five-membered cyclic peroxide in Ni-ARD (*22*).

The XAS data presented here provide detailed structural information regarding the Ni sites in the resting Ni-ARD and ES complexes and establish key steps in the early part of the mechanism (Scheme 2). The structure of resting Ni-ARD that emerges from the analysis of XAS data is that of a six coordinate Ni site composed of O/N-donor ligands, of which 3−4 are His imidazole rings. Although it is not possible to completely rule out the presence of a single S-donor on the basis of EXAFS analysis alone (see Table S1), the EXAFS is clearly not dominated by S-scattering atoms, as is the case in other Ni-containing metalloenzymes that catalyze redox reactions (vide infra). Furthermore, the proposed structure is corroborated by the facts that (i) the amino acid sequence of the protein contains seven His residues, of which three are invisible in the NMR spectrum because of paramagnetic effects arising from a high-spin ($S = 1$) Ni^{2+} center (*21*), (ii) there is no electronic absorption in the resting enzyme below 300 nm (*24*) that would be

Scheme 2

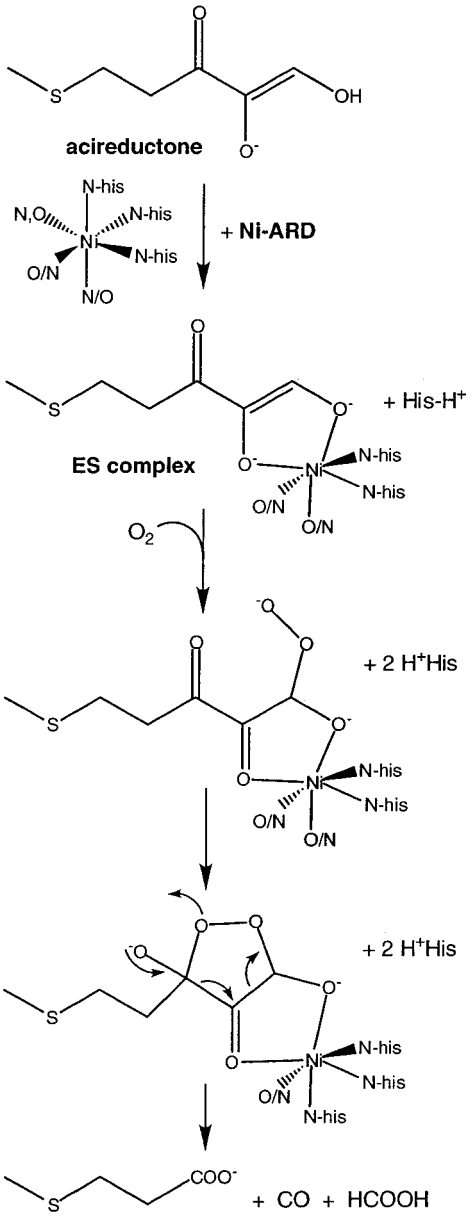

expected for a thiolate ligand (S → Ni LMCT), and (iii) the ongoing refinement of the solution structure of Ni-ARD using NMR shows that both Cys residues are observed; therefore, neither lies close enough to the paramagnetic Ni center to be a ligand (*25*).

The structure of the Ni-ARD ES complex also reveals a six coordinate Ni center, but the spectrum is quite distinct from that obtained on the resting enzyme (Figure 2). Analysis of the EXAFS data is consistent with a higher O-donor content in the first coordination sphere of Ni in the ES complex. The data are best fit with two short O(/N)-donor ligands, implying a bidentate binding mode for the substrate. This is consistent with expectations from the structure of acireductone, which reveals that it could bind to the metal as a dianion in a bidentate fashion forming a five-membered catecholate-like chelate ring with the Ni center (Scheme 2) and consistent with the electronic absorption spectral changes that occur when substrate binds to Ni-ARD (vide supra). Because the resting enzyme contains a Ni center that is coordinately saturated, this would require the substitution of two ligands. Comparison of the EXAFS data for the resting Ni-ARD and the ES complex show that at least one of these displaced ligands is a histidine. It is possible that this histidine ligand is the base used to deprotonate the substrate to form the dianion. It is also possible that the short 1.9 Å Ni−O distance observed in the resting enzyme arises from coordination of OH^-, which could also serve as the base involved.

Dioxygenases exhibit two limiting mechanisms, both of which are exemplified by mononuclear, nonheme, Fe-containing dioxygenases (*26*). In the first mechanism, the enzyme employs a reduced, redox active metal, Fe^{2+}, to activate dioxygen for subsequent oxidation of the substrate. In the second mechanism, the metal serves to activate the substrate toward reaction with O_2. This appears to be the case for dioxygenases that require Fe^{3+}. The former mechanism requires a redox active metal capable of reducing O_2, while the latter mechanism does not require a change in the redox state of the metal. It relies on ligand-to-metal charge transfer to activate the substrate. The use of Ni^{2+} in a dioxygenase to activate O_2 toward reaction with a substrate is unexpected from the standpoint that Ni^{2+} in an O/N-rich ligand environment does not typically have biologically accessible redox chemistry. On the basis of structural studies of other redox active Ni-containing metalloenzymes (*27*, *28*) (e.g., hydrogenase (*10*, *29*−*31*), superoxide dismutase (*32*), and CO-dehydrogenase (*33*)), cysteine thiolate ligation would be expected in order to generate an accessible Ni(III/II) redox couple. The XAS characterization of Ni-ARD shows no evidence of the requisite cysteine thiolate ligation and no evidence of redox state change upon substrate binding and is therefore consistent with a nonredox role for the Ni center. Except for the lack of Ni redox chemistry, the absence of Cys ligation in the active site of NiARD is not unexpected for a dioxygenase, since thiolates are sensitive to oxidation by dioxygen and no example of a dioxygenase featuring Cys ligation of the metal center is known (*26*).

There is yet little concrete data about differences between the differing activities of the Fe-ARD and Ni-ARD enzymes, although metal replacement experiments indicate that Fe-ARD activity can be reconstituted in apo-ARD by addition of Mg(II), another nonredox active metal ion (*24*). As such, it appears unlikely that the activity differences between Fe- and Ni-ARD arise from the presence of a redox active center vs a nonredox active center. On the other hand, it is noteworthy that the C−C bond cleaved in Fe catechol dioxygenases is mechanism-dependent (*26*). Those enzymes that are active with Fe^{2+} and employ redox activation of O_2 exhibit extradiol cleavage (e.g., 2,3-dihydroxybiphenyl 1,2-dioxygenase), while Fe^{3+}-dependent enzymes exhibit intradiol cleavage (e.g., catechol 1,2-dioxygenase, protocatachuate 3,4-dioxygenase). The change in regiospecificity has been associated with a change in the reactive O_2 species from Fe-generated nucleophilic superoxide ion to electrophilic dioxygen (*26*).

In the current case, the different regiochemistries exhibited by Fe-ARD and Ni-ARD may be attributable to changes in the nature of the ligated species formed in the ES complex. We are currently investigating the use of NMR methods to characterize the metal-bound substrate species in more detail, in the hope that this will provide insight into the precise nature of the substrate bound in the ES complex.

ACKNOWLEDGMENT

T.C.P. and T.J. thank Dr. Susan Sondej Pochapsky for her expert assistance in obtaining and processing the NMR data and Dr. Huaping Mo for access to his NMR data on Ni-ARD.

SUPPORTING INFORMATION AVAILABLE

Tables S1 and S2 of curve-fitting results of filtered EXAFS spectra of the *Klebsiella pneumoniae* NiARD resting enzyme and ES complex, respectively. This material is available free of charge via the Internet at http://pubs.acs.org.

REFERENCES

1. Wolfe, S. L. (1993) *Molecular and Cellular Biology*, Wadsworth, Belmont.
2. Schlenk, F. (1983) in *Advances in Enzymology* (Meister, A., Ed.) pp 195−266, Wiley and Sons, New York.
3. Shapiro, S. K., and Barrett, A. (1981) *Biochem. Biophys. Res. Commun. 102*, 302−307.
4. Wray, J. W., and Abeles, R. H. (1995) *J. Biol. Chem. 270*, 3147−3153.
5. Dai, Y., Wensink, P. C., and Abeles, R. H. (1999) *J. Biol. Chem. 274*, 1193−1195.
6. Myers, R. W., Wray, J. W., Fish, S., and Abeles, R. H. (1993) *J. Biol. Chem. 268*, 24785−24791.
7. Perreaux, D., Maraite, H., and Meyer, J. A. (1986) *Physiol. Mol. Plant Pathol. 28*, 323−328.
8. Brann, D. W., Bhat, G. K., Lamar, C. A., and Mahesh, V. B. (1997) *Neuroendocrinology 65*, 385−395.
9. Verma, A., Hirsch, D. J., Glatt, C. E., Ronnett, G. V., and Snyder, S. H. (1993) *Science 259*, 381−384.
10. Bagyinka, C., Whitehead, J. P., and Maroney, M. J. (1993) *J. Am. Chem. Soc. 115*, 3576−85.
11. Colpas, G. J., Maroney, M. J., Bagyinka, C., Kumar, M., Willis, W. S., Suib, S. L., Mascharak, P. K., and Baidya, N. (1991) *Inorg. Chem. 30*, 920−928.
12. Ressler, T. (1997) *J. Phys. IV 7*, C2−269.
13. Stewart, J. M., Lingafelter, E. C., and Breazeale, J. D. (1961) *Acta Crystallogr. 14*, 888−891.
14. van Ingen Schenau, A. D. (1975) *Acta Crystallogr. B31*, 2736−2738.
15. Rosenfield, S. G., Armstrong, W. H., and Mascharak, P. M. (1986) *Inorg. Chem. 25*, 3014−3018.
16. Davidson, G., Clugston, S. L., Honek, J. F., and Maroney, M. J. (2001) *Biochemistry 40*, 4569−4582.
17. Eidsness, M. K., Sullivan, R. J., and Scott, R. A. (1988) in *The Bioinorganic Chemistry of Nickel* (Lancaster, J. R., Jr., Ed.) pp 73−91, VCH, New York.
18. Liu, W., and Thorp, H. H. (1993) *Inorg. Chem. 32*, 4102−4105.
19. Hannan, J. P., Whittaker, S. B.-M., Hemmings, A. M., James, R., Kleanthous, C., and Moore, G. R. (2000) *Inorg. Biochem. 79*, 365−370.
20. Bertini, I., Canti, C., Luchinat, C., and Mani, F. (1981) *J. Am. Chem. Soc. 103*, 7784−7788.
21. Mo, H., Dai, Y., Pochapsky, S. S., and Pochapsky, T. C. (1999) *J. Biomol. NMR 14*, 287−288.
22. Dai, Y., Pochapsky, T. C., and Abeles, R. H. (2001) *Biochemistry 40*, 6379−6387.
23. Wray, J. W., and Abeles, R. H. (1993) *J. Biol. Chem. 268*, 21466−21469.
24. Dai, Y. (1999) in *Biochemistry*, Brandeis University, Waltham.
25. Pochapsky, T. C., unpublished results.
26. Que, L., Jr., and Ho, R. Y. (1996) *Chem. Rev. 96*, 2607−2624.
27. Maroney, M. J., Davidson, G., Allan, C. B., and Figlar, J. (1998) *Struct. Bonding 92*, 1−65.
28. Maroney, M. J. (1999) *Curr. Opin. Chem. Biol. 3*, 188−199.
29. Volbeda, A., Charon, M. H., Piras, C., Hatchikian, E. C., Frey, M., and Fontecilla-Camps, J. C. (1995) *Nature 373*, 580−587.
30. Volbeda, A., Garcin, E., Piras, C., de Lacey, A. L., Fernandez, V. M., Hatchikian, E. C., Frey, M., and Fontecilla-Camps, J. C. (1996) *J. Am. Chem. Soc. 118*, 12989−12996.
31. Davidson, G., Choudhury, S. B., Gu, Z. J., Bose, K., Roseboom, W., Albracht, S. P. J., and Maroney, M. J. (2000) *Biochemistry 39*, 7468−7479.
32. Choudhury, S. B., Lee, J.-W., Davidson, G., Yim, Y.-I., Bose, K., Sharma, M. L., Kang, S.-O., Cabelli, D. E., and Maroney, M. J. (1999) *Biochemistry 38*, 3744−3752.
33. Dobbek, H., Svetlitchnyi, V., Gremer, L., Huber, R., and Meyer, O. (2001) *Science 293*, 1281−1285.

BI012209A